*Ab initio* study on the electronic structure and vibration modes of alkali and alkaline-earth amides and alanates



2009 J. Phys.: Condens. Matter 21 185501

(http://iopscience.iop.org/0953-8984/21/18/185501)

J. Phys.: Condens. Matter **21** (2009) 185501 (9pp) doi:10.1088/0953-8984/21/18/185501

# *Ab initio* study on the electronic structure and vibration modes of alkali and alkaline-earth amides and alanates

**Takao Tsumuraya**[1], **Tatsuya Shishidou**[1] **and Tamio Oguchi**[1,2]

[1] Department of Quantum Matter, ADSM, Hiroshima University, Higashihiroshima 739-8530, Japan
[2] Institute for Advanced Materials Research, Hiroshima University, Higashihiroshima 739-8530, Japan

Received 3 March 2009
Published 31 March 2009
Online at stacks.iop.org/JPhysCM/21/185501

**Abstract**
We study the electronic structure and vibrational modes of several amides $M(NH_2)_n$ and alanates $M(AlH_4)_n$ (M = K, Na, Li, Ca and Mg), focusing on the role of cation states. Calculated breathing stretching vibration modes for these compounds are compared with measured infrared and Raman spectra. In the amides, we find a significant tendency such that the breathing mode frequencies and the structural parameters of $NH_2$ vary in accordance with the ionization energy of cation. The tendency may be explained by the strength in hybridization between cation orbitals and molecular orbitals of $(NH_2)^-$. The microscopic mechanism of correlations between the vibration frequencies and structural parameters is elucidated in relation to the electronic structure. A possible similar tendency in the alanates is also discussed.

(Some figures in this article are in colour only in the electronic version)

## 1. Introduction

Hydrogen has great potential as an energy source. The development of a hydrogen storage system is one of the major challenges related to the utilization of hydrogen as a significant energy carrier in the near future [1, 2]. Solid state storage is recognized to be the safest and most reliable approach for this purpose [3]. Recently, light alkaline and alkaline-earth metal hydrides have attracted growing interest as reversible hydrogen storage materials because of their innately high hydrogen content. Among them, the complex metal hydrides with chemical formula $M(AH_x)_n$ seem most promising, where M is an alkaline or alkaline-earth metal ion ($n = 1$ for M = K, Na and Li, $n = 2$ for M = Ca and Mg) and A represents Al, B ($x = 4$) and N ($x = 2$). $M(NH_2)_n$, $M(AlH_4)_n$ and $M(BH_4)_n$ are called amides, alanates and borohydrides, respectively [4–6]. However, at present, no material fulfills all requirements for on-board vehicular hydrogen storage, such as low operational temperature of hydrogen desorption and low pressure of hydrogen absorption reaction, rapid kinetics and reversibility. Many fundamental scientific and technological challenges still remain. The bonding nature and crystal structure of these materials are of broad interest and fundamental importance for understanding the properties of materials [7–12]. The crystal structure is generally unique for each complex hydride. One of the common interesting features of these complex hydrides is that the electronic structure can be considered as an ionic solid phase [13–15]. This means that they are comprised of a metal cation $M^{n+}$ and anionic complexes such as $(NH_2)^-$, $(AlH_4)^-$ and $(BH_4)^-$. Recently, the crystal structure of mixed cations and/or anions such as $Li_2BNH_6$, $Li_4BNH_{10}$, $Li_2Mg(NH)_2$ and $Li_2Ca(NH)_2$ have been studied by using neutron and synchrotron x-ray powder diffraction measurements [16–19] and by a first-principles calculation [20]. Hydrogen absorption and desorption properties are also unique for each system, depending on the combination of different cations and anions. For instance, Chen *et al* [4] originally proposed a novel reversible hydrogen storage reaction where lithium amide $LiNH_2$ reacts with lithium hydride LiH:

$$LiNH_2 + LiH \longleftrightarrow Li_2NH + H_2. \quad (1)$$

Unfortunately, the desorption reaction requires a temperature higher than 230 °C at an equilibrium hydrogen pressure of 1 atm. This reaction temperature is too high for vehicular applications. In an effort to lower the equilibrium temperature

 

**Table 1.** Crystal structure of amides $M(NH_2)_y$.

| | Space group | $a$ (Å) | $b$ (Å) | $c$ (Å) |
|---|---|---|---|---|
| $KNH_2$ [38] | $P2_1/m$ | 4.5487 | 3.7631 | 6.1894 |
| $NaNH_2$ [39] | $Fddd$ | 8.949 | 10.456 | 8.061 |
| $LiNH_2$ [40] | $I\bar{4}$ | 5.048 | | 10.278 |
| $Ca(NH_2)_2$ [41] | $P2_1/a$ | 6.30 | 7.257 | 7.2434 |
| | | | | $\gamma = 124.73°$ |
| $Mg(NH_2)_2$ [36] | $I4_1/acd$ | 10.3779 | | 20.065 |

**Table 2.** Crystal structure of alanates $M(AlH_4)_y$.

| | Space group | $a$ (Å) | $b$ (Å) | $c$ (Å) |
|---|---|---|---|---|
| $KAlH_4$ [42] | $Pnma$ | 8.8249 | 5.8590 | 7.3872 |
| $NaAlH_4$ [43] | $I4_1/a$ | 4.99 | | 11.70 |
| $LiAlH_4$ [44] | $P2_1/a$ | 7.825 | 4.837 | 7.809 |
| | | | | $\gamma = 112.137°$ |
| $Ca(AlH_4)_2$ [45] | $Pbca$ | 13.37 | 9.28 | 8.91 |
| $Mg(AlH_4)_2$ [46] | $P\bar{3}m1$ | 5.18 | | 5.98 |

and/or raise the equilibrium pressure, several groups have independently investigated cation substitutions by varying ratios of $Mg(NH_2)_2$, $Ca(NH_2)_2$, $MgH_2$ or $CaH_2$ [21–26]. They have found that hydrogen desorption starts at temperatures as low as 150 °C. However, the reason for decreasing the hydrogen desorption temperature and the role of cations in the reaction remain unknown [27–29]. Although a number of extensive experimental and theoretical works have been carried out for such materials, the hydrogenating and dehydrogenating reaction mechanisms and properties of materials are still a remaining issue to be investigated. In particular, the role of cation states in the electronic and crystal structure has not been well identified yet.

In this study, the electronic structure of several amides and alanates with different cations is investigated by first-principles density functional calculations. Especially focusing on the role of cation states, we investigate the breathing stretching vibration modes of N–H in the amides and Al–H in the alanates, and compare them with the measured infrared (IR) [30–32] and Raman spectra [33]. We find that the vibration frequencies of the breathing mode and the structural parameters of $NH_2$ and $AlH_4$ are correlated with the ionization energy of the cation. Furthermore, a systematic trend can also be seen in the hybridization between cation orbitals and molecular orbitals of $(NH_2)^-$ and $(AlH_4)^-$. We elucidate the microscopic mechanism of correlations between the breathing mode frequencies of N–H and Al–H and structural parameters by analyzing the calculated electronic structure from a molecular-orbital point of view.

## 2. Crystal structure

The alkaline and alkaline-earth metal amides and alanates display a rich variety of physical properties and hydrogen desorption properties. The amide is defined as a compound derived from ammonia by replacement of a hydrogen atom with an electron of a cation, containing the $(NH_2)^-$ anion. The structures of $LiNH_2$ and $Mg(NH_2)_2$ are body-centered tetragonal and $NaNH_2$ has an orthorhombic structure. For all of them, there is a pseudo-fcc packing of nitrogen. Cations are all surrounded by the $(NH_2)^-$ anions: Li, Na and Mg are nearly tetrahedrally, and K and Ca are nearly octahedrally, coordinated. The bond length and angle of the $(NH_2)^-$ anion in the amides are quite similar to those of the iso-electronic $H_2O$ molecule (O–H bond length 0.957 Å and H–O–H bond angle 104.47° [34]). In the crystal structure of the alanates, the local geometry of $AlH_4$ molecules takes a tetrahedral configuration. Alanates show a similar crystal structure to that of the aforementioned amides. Li, Na and Mg are nearly tetrahedrally coordinated, and K and Ca are nearly octahedrally coordinated by $(AlH_4)^-$. The $AlH_4$ complexes in the compounds are slightly distorted from the ideal tetrahedral geometry because of bulk environment. The bond distance between Al and H is about 1.6 Å. For the crystal structure of $Ca(AlH_4)_2$, the $CaB_2F_8$ type is known as the stable phase, but several phases competitive in energy have been suggested from the first-principles calculation by Wolverton *et al* [35].

In the present work, the internal atomic positions of each compound are optimized via atomic-force calculations. Regarding the space group and lattice constants, we use the experimentally determined one [36, 37], which are listed in table 1 for the amides and in table 2 for the alanates.

## 3. Methods

The present first-principles calculations are performed by adopting the all-electron full-potential linear augmented plane wave (FLAPW) method [47–52] based on the density functional theory [53, 54] within the generalized gradient approximation (GGA) [55]. Kohn–Sham equations are solved self-consistently in a scalar-relativistic manner. Uniform $k$-mesh sets of $4 \times 4 \times 4$ for $LiNH_2$, $KNH_2$, $NaNH_2$, $Ca(NH_2)_2$, $LiAlH_4$, $KAlH_4$, $NaAlH_4$ and $Mg(AlH_4)_2$, $3 \times 3 \times 3$ for $Mg(NH_2)_2$ and $2 \times 2 \times 2$ for $Ca(AlH_4)_2$ are used for the integration in the Brillouin zone of each structure. Muffin-tin sphere radii are set to be 0.55 and 1.0 Å for N and Al, respectively for all compounds. The spherical radius of H is taken to be 0.55 Å for all alanates and 0.35 Å for all amides. The spherical radii of cations are set to be 1.0 Å for K, Mg and Ca, 0.9 Å for Na and 0.8 Å for Li. The plane wave cutoffs are 30 and 300 Ryd in the amides and 25 and 200 Ryd in the alanates for the LAPW basis functions, and the potential and charge density, respectively. The breathing mode is calculated by the frozen phonon technique with small atomic displacements of H, ±0.01 Å in the amides and ±0.02 Å in the alanates. To get the breathing mode of $Mg(NH_2)_2$, which has quite a large unit cell, we relied on the ultrasoft-pseudopotential method, by using the STATE (simulation tool for atom technology) code [56–58]. There the plane wave cutoffs are 36 and 324 Ryd for the wavefunction and the charge density, respectively, and $4 \times 4 \times 4$ $k$-mesh points are used for the calculation.

## 4. Results and discussions

### *4.1. Amides $M(NH_2)_n$*

The isolated $NH_2$ molecule belongs to the point group $C_{2v}$ (2 mm). There are three vibration modes for the $NH_2$ molecule: the breathing mode with $A_1$ symmetry $\nu_1$, in which only the bond length is changed, the bending mode with $A_1$ symmetry $\nu_2$ and the asymmetric stretching mode with $B_2$ symmetry $\nu_3$. All modes are IR-and Raman-active [59]. Among them, we focus on the breathing stretching modes $\nu_1$. Figure 1 shows calculated N–H breathing modes in the amides with different cations. It is found that the calculated frequencies are increased as the ionization energy of the cations is increased. Optimized interatomic distances between N and H and angles of $NH_2$ in the amides are also presented in figure 1. The interatomic distances between N and H are decreased and the bond angles of H–N–H are increased as the ionization energy of the cations is increased. These tendencies are the main issues to be investigated in the present study.

Measured IR spectra of several amides and imides were originally reported by Linde *et al* [30]. The amides exhibit two sharp bands in their IR spectrum corresponding to N–H stretches around 3200–3400 $cm^{-1}$. They have observed that small but significant differences are found in the symmetric and asymmetric stretching modes of $NH_2$ molecules in the amides, depending on the cations. Bohger *et al* [33] have investigated the IR and Raman spectra of $LiNH_2$. They have reported that the frequency of the breathing mode $\nu_1$ (3258 $cm^{-1}$) is slightly lower than the asymmetric stretching modes $\nu_3$ (3310 and 3315 $cm^{-1}$). Our calculated frequencies of the breathing mode $\nu_1$ are 3208 and 3226 $cm^{-1}$, as shown in the bottom panel of figure 1. The calculated values are consistent with the results of the previous first-principles calculation based on the ultrasoft-pseudopotential method by Herbst *et al* [62] (3286–3306 and 3379–3386 $cm^{-1}$). The corresponding breathing modes $\nu_1$ measured by IR or Raman absorption spectra for the amides are also represented in the bottom panel of figure 1.

Let us discuss the tendencies by considering the electronic structure of the amides. Figures 2(a)–(e) show the calculated density of states (DOS) of $LiNH_2$. The partial DOSs projected on cation orbitals are generally quite small within the cation muffin-tin spheres in the valence and conduction band regions (see figure 2(e)). The valence bands are composed mostly of N s and p and H s states (see figures 2(b)–(d)). These results show that the amide may have almost an ionic electronic structure of $M^{n+}$ and $(NH_2)^-$.

In $AH_2$ molecules, there are two possible types of geometry in general. One is the bent structure with $C_{2v}$ symmetry. The other is the linear $D_{\infty h}$ structure. Figure 3 shows the molecular orbitals of $AH_2$ with linear and bent geometries. In a four-electron system such as $BeH_2$, the linear geometry is more stable than the bent one. An eight-electron system takes a bent geometry like $H_2O$ since the $2a_1$ molecular orbital in the bent structure is lower in energy than the $\pi_u$ orbitals in the linear geometry. The most interesting thing is that the $2a_1$ orbital is a linear combination of $2\sigma_g$ and one of $\pi_u$ in the linear geometry. In the case of the electronic structure of amides, the cation gives one electron

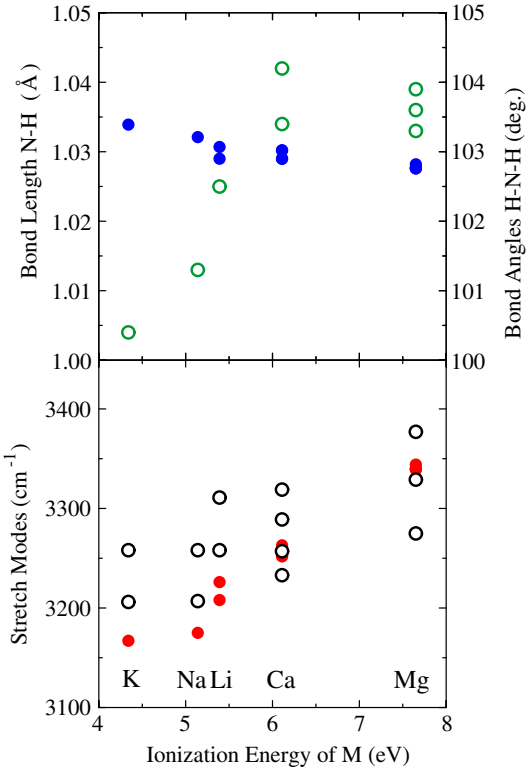


**Figure 1.** Bottom panel: red dots represent calculated breathing mode $\nu_1$ of amides $M(NH_2)_y$. Black open circles denote measured IR or Raman frequency of stretching mode [30, 33, 60]. It should be noted that these measured values include both symmetric $\nu_1$ and asymmetric $\nu_3$ modes. In general, the symmetric frequency of $\nu_1$ can be considered as slightly lower than the asymmetric stretching modes $\nu_3$. Top panel: blue dots represent optimized N–H bond lengths and green open circles denote our optimized bond angles of $NH_2$ in amides. Ionization energies of M (eV) are taken from [61].

to the $NH_2$ molecule, leading to eight electrons occupying the molecular orbitals of $NH_2$. So, the $NH_2$ geometry in the amides definitely prefers to be bent. In this context, the general features in DOS of the amides in figures 2(b)–(d) can be understood by a schematic energy diagram described with bent $AH_2$ molecular-orbital models for the isolated amide molecule illustrated in figure 2(f). Total charge density and each molecular orbital of an isolated $(NH_2)^-$ molecule are illustrated in figures 2(g)–(k). There are four states occupied with eight electrons. The lowest occupied state (figure 2(k)) is the $1a_1$ bonding state between N s and H s, and its anti-bonding counterpart is the third occupied state (figure 2(i)), which has a lone-pair predominantly made of N p orbitals with the $a_1$ irreducible representation. The highest occupied state in $(NH_2)^-$ (figure 2(h)) is non-bonding, consisting of N $p_\pi$ orbitals.

We now look at a feature in the electronic structure for the amides with different cations. Figure 4 shows calculated partial DOS of cations in the amides. DOSs of the amides with different cations in the valence band region are similar to those of $LiNH_2$ (figures 2(a)–(e)). However, we can see a significant difference in the calculated partial DOS of cations. The magnitude of hybridization between cation orbitals and the molecular orbitals of $(NH_2)^-$ leads to a difference in the

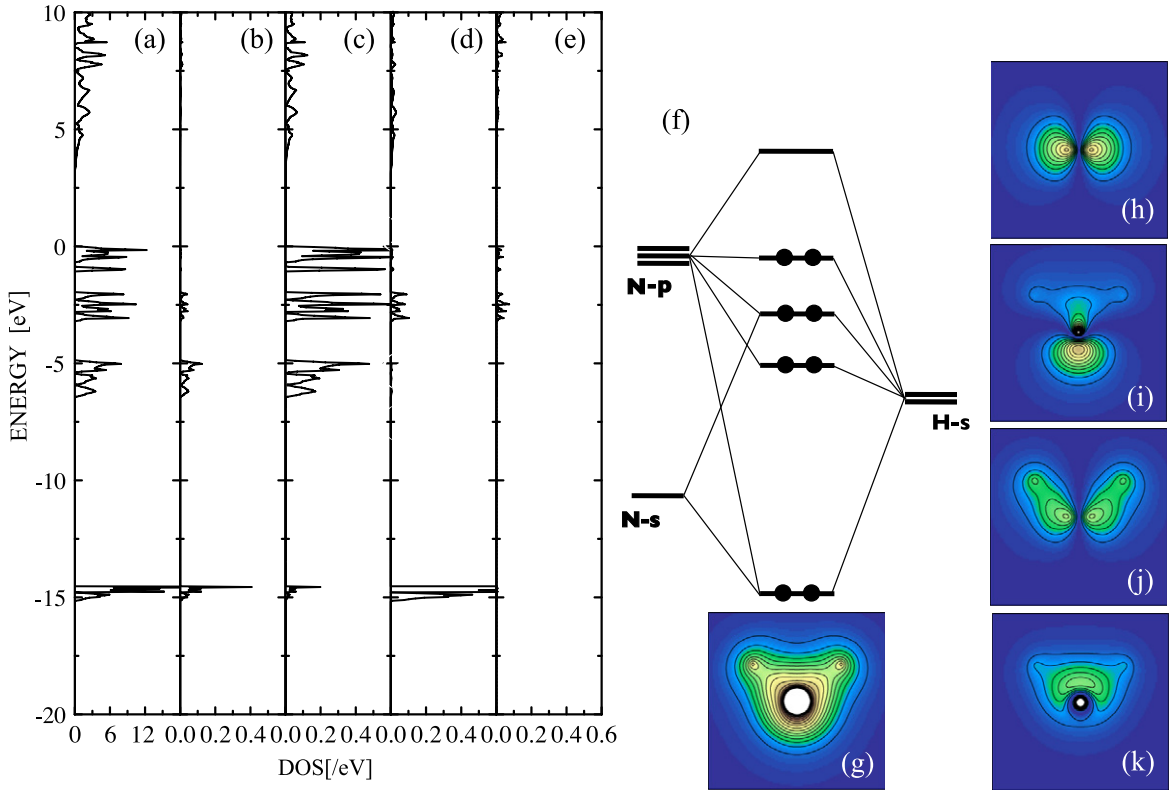


**Figure 2.** (a) Calculated total density of states (DOS) of $LiNH_2$ and partial DOS of $LiNH_2$: (b) H s, (c) N p, (d) N s, (e) Li s and p. The energy zero is set to be at the valence band maximum in all DOS. (f) Schematic energy diagram of the molecular orbitals of $NH_2$ where dots represent electrons occupying the molecular orbitals in the case of an eight-electron system like $H_2O$. (g) Total charge density of an isolated $(NH_2)^-$ molecule which is decomposed into the contributions from each molecular orbital (h)–(k) which is shown in the $xy$ plane. Only in (h) is the molecular orbital shown in the $yz$ plane perpendicular to the H–N–H plane.

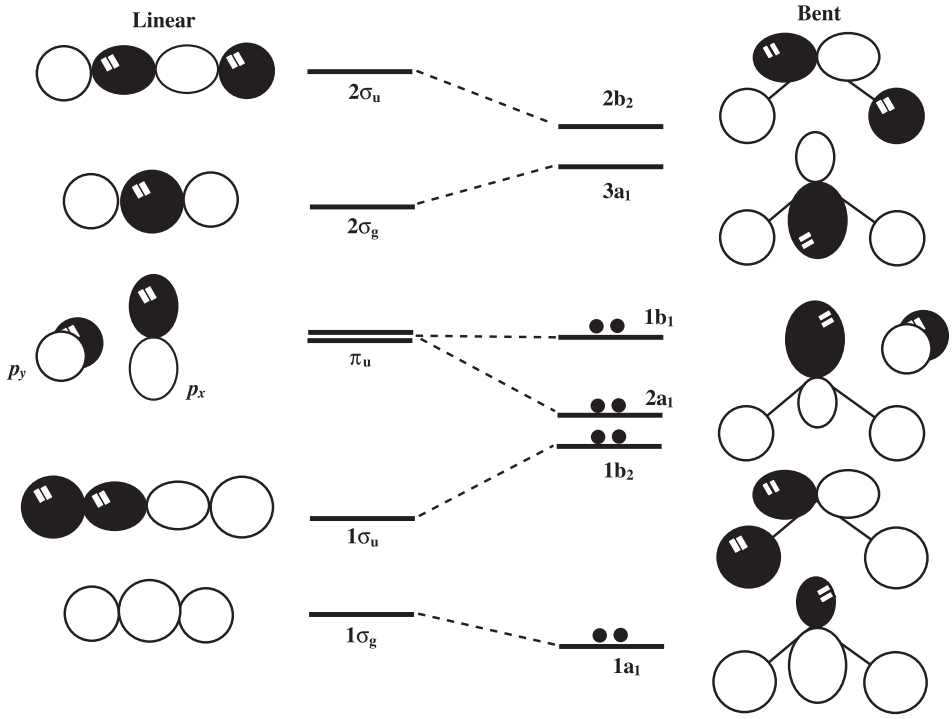


**Figure 3.** Schematic energy diagram and molecular orbitals of an $AH_2$ molecule with linear and bent geometries. Dots represent electrons occupying the molecular orbitals in the case of an eight-electron system like $H_2O$.

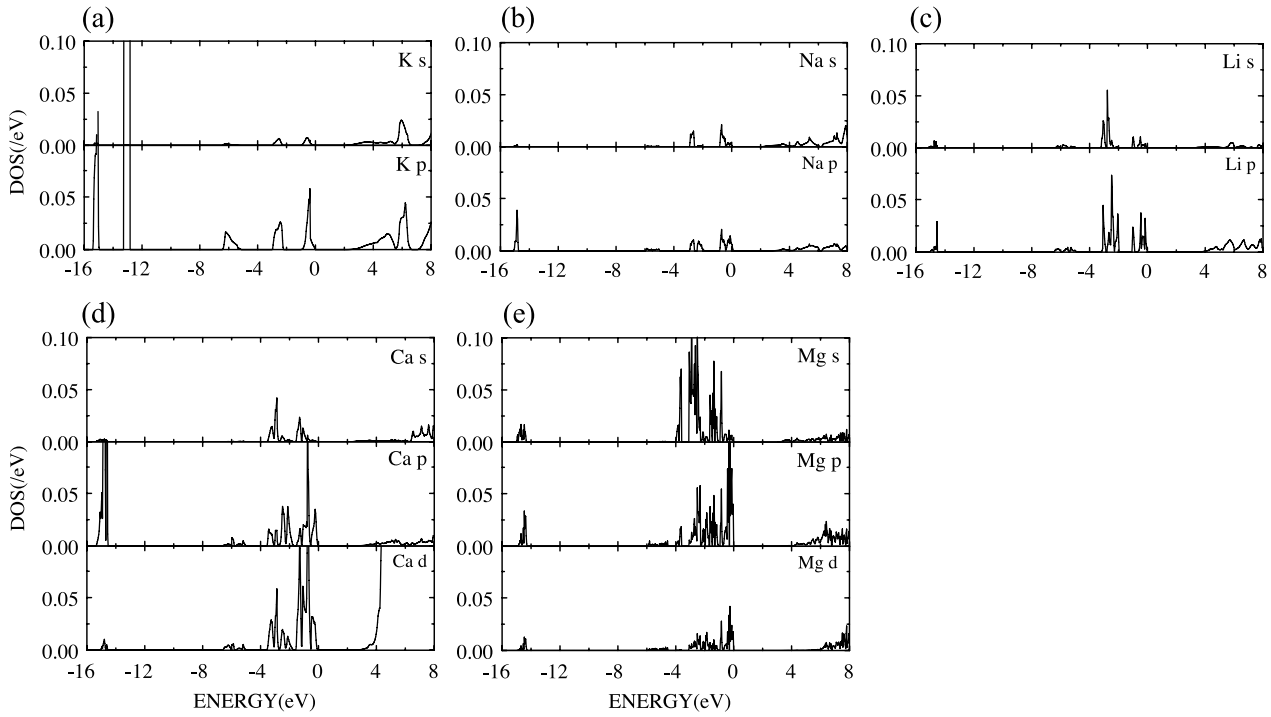


**Figure 4.** Cation partial DOS of amides with different cations. The energy zero is set to be at the valence band maximum. (a) $KNH_2$, (b) $NaNH_2$, (c) $LiNH_2$, (d) $Ca(NH_2)_2$, (e) $Mg(NH_2)_2$.

valence band partial DOS. The occupied fraction of the cation is almost proportional to the ionization energy of the cation, which may be a measure of the highest occupied energy level position in a neutral atom case. That is to say, the covalency is slightly introduced into the ionic bonding between $M^{n+}$ and $(NH_2)^-$. As can seen be in the partial DOS of the cations, the cation orbitals are hybridized significantly with the third (the second highest) occupied states $2a_1$ of the molecular orbitals, which have an anti-bonding character between N s and H s and is composed of $\pi_u$ and $2\sigma_g$ components in the linear geometry (see figure 3). Such cation hybridization introduces less occupancy in $2a_1$ and consequently in $2\sigma_g$, resulting in stronger bonding and slightly less bending. In other words, the occupancy reduction in the $2a_1$ molecular orbital moves the molecular stability towards a linear geometry. Therefore, the tendency found in the breathing mode frequencies, bond lengths and bond angles can be understood by the occupancy reduction in the lone-pair $2a_1$ molecular orbital in $(NH_2)^-$ introduced by the cation hybridization.

### *4.2. Alanates $M(AlH_4)_n$*

A tetrahedral hydride $AH_4$ has four normal modes of vibration [59]. All four vibrational modes are Raman-active, whereas only asymmetric stretching modes ($F_2$ symmetry) $\nu_3$ and $\nu_4$ are IR-active. Thus, it should be noted that the main structure in a frequency region of 1600–2000 $cm^{-1}$ in the IR spectra is an asymmetric $\nu_3$ mode. On the other hand, the main structure in a frequency region of 1600–2000 $cm^{-1}$ in the Raman spectra is a symmetric mode $\nu_1$. The $\nu_1$ mode is the breathing stretching one of Al–H bonds, which keeps the tetrahedral symmetry unchanged, since it belongs to the full

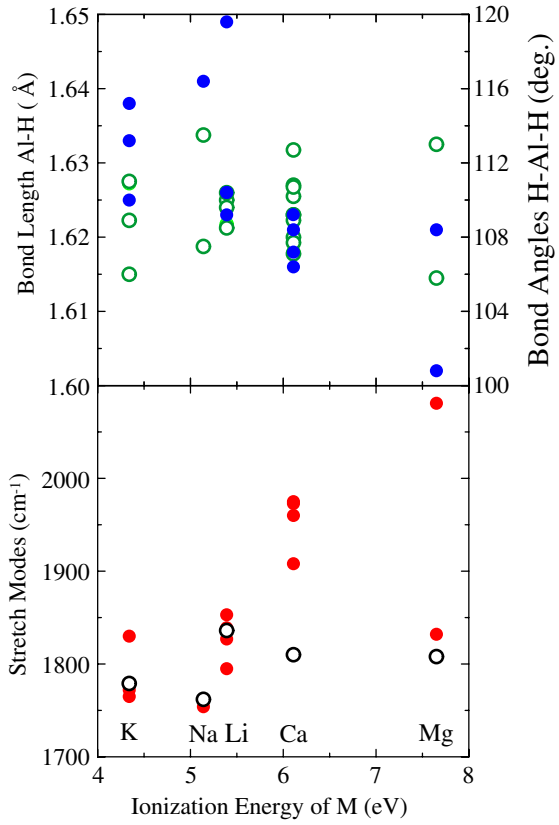


**Figure 5.** Bottom panel: red dots represent calculated breathing mode frequencies of alanates $M(AlH_4)_y$. Black open circles denote measured breathing mode frequencies after [63–65]. Top panel: blue dots represent optimized N–H bond lengths and green open circles denote optimized angles of H–Al–H in alanates. Ionization energies of M (eV) are taken from [61].

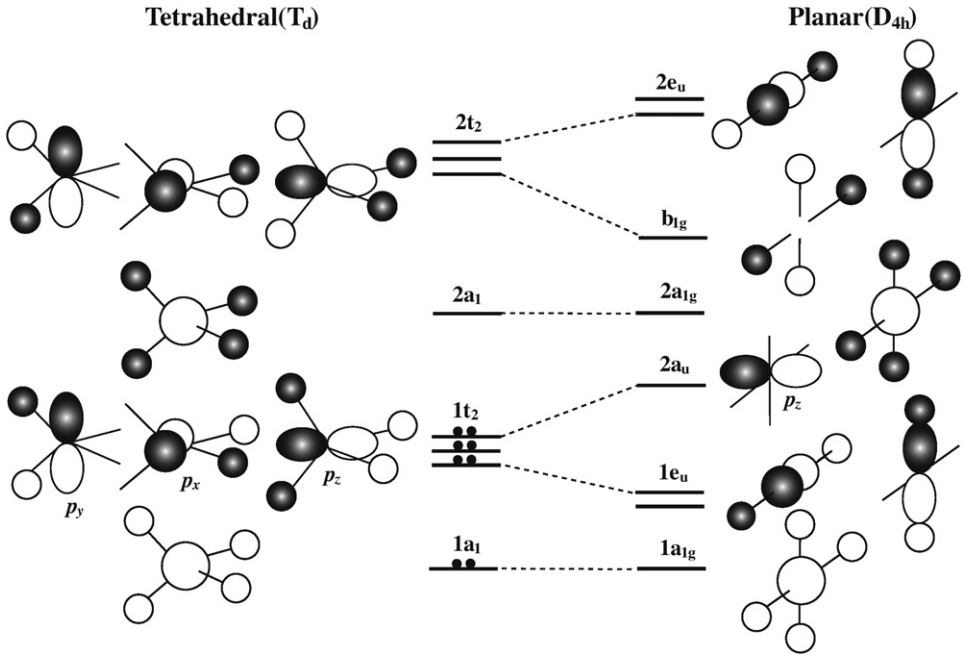


**Figure 6.** Schematic energy diagram of the molecular orbital of an $AH_4$ molecule with tetrahedral and square planar geometries. Dots represent electrons occupying the molecular orbitals in the case of an eight-electron system like $CH_4$.

symmetric $A_1$ irreducible representation. The frequency of the $\nu_1$ mode is slightly higher than that of the $\nu_3$ mode. Our calculated frequencies of the breathing mode $\nu_1$ of the alanates are plotted in the bottom panel of figure 5, together with the corresponding data obtained from measured Raman absorption spectra. We found that the frequencies of the breathing modes are increased and the bond distances between Al and H are decreased, in proportion to the ionization energy of the cations. However, the H–Al–H bond angles in our optimized alanate structure reveal no clear tendencies as shown in the top panel of figure 5. Thus, it can be considered that there are at least two factors to determine the structural parameters of $AlH_4$. One is that the breathing mode frequencies of Al–H and structural parameters can be explained by the molecular orbitals of $AlH_4$ and the trend is governed by the hybridization of the cation states. The other factor may be direct effects by cation to hydrogen because of longer Al–H bond lengths. Although, in the amide, the nearest-neighbor atoms from cations are nitrogen, in the alanates that of cation is hydrogen; bonding distances between cation and hydrogen are ranging from 1.8 to 2.8 Å, depending on the ionic radius of the cation.

From the view of molecular orbitals of $AlH_4$, the following microscopic mechanism can be considered. There are two geometries that we often see for the structure of $AH_4$. One is that A is tetrahedrally coordinated by H with $T_d$ symmetry. The other is a square planar structure with $D_{4h}$ symmetry. Figure 6 shows a schematic energy diagram described with the molecular orbitals of tetrahedral $T_d$ (left panel) and planar square $D_{4h}$ (right panel) geometries of $AH_4$. In the molecular orbitals of the tetrahedral $T_d$ geometry, there is the bonding state with $1t_2$ irreducible representation made of triply degenerated p orbitals ($p_x$, $p_y$, $p_z$) of *A* mixing with four H s orbitals. If H atoms move to a planar square $D_{4h}$ geometry, the $1t_2$ orbitals split into doubly degenerated orbitals ($1e_u$) and a non-degenerated one ($2a_u$). The latter in the square planar $D_{4h}$ geometry cannot mix with any H orbital. In a six- or seven-electron system, the square planar $D_{4h}$ configuration is more stable than the tetrahedral $T_d$ one. It turns out that, in an eight-electron system, the tetrahedral $T_d$ configuration becomes relatively more stable. In the electronic structure of alanates, a cation donates one electron to an $AlH_4$ molecule. Thus, eight electrons occupy the molecular orbitals of $AlH_4$. The local structure of $AlH_4$ molecules in the alanates takes a tetrahedral configuration. Calculated DOS of $NaAlH_4$ are shown in figures 7(a)–(f). The valence bands are composed mostly of Al s and p and H s states. All alanates have almost ionic bonding of $M^{n+}$ and $(AlH_4)^-$ and DOSs in the valence band region are quite similar to each other. The general features in DOS can be understood by a schematic energy diagram describing a tetrahedral $AH_4$ molecular-orbital model illustrated in figure 7(g). Total charge density and each molecular orbital of an isolated $(AlH_4)^-$ molecule are represented in figures 7(h)–(l). Figure 8 represents partial DOS of cations in the alanates. A similar tendency to the case of amides with a different cation can also be seen in the cation partial DOS of the alanates. As can be seen in the partial DOS, cation orbitals are hybridized mostly with the $1t_2$ molecular orbital at the highest occupied states. An enhancement of the hybridization between cation and $1t_2$ orbitals results in the reduction of the occupied fraction in the highest occupied molecular orbital. That is to say, the covalency is certainly introduced into the ionic bonding.

It can be expected that the occupancy reduction in the $1t_2$ molecular orbital brings a stability shift toward the planar square structure. Thus, the $AlH_4$ geometry might be slightly distorted from the ideal tetrahedral toward the

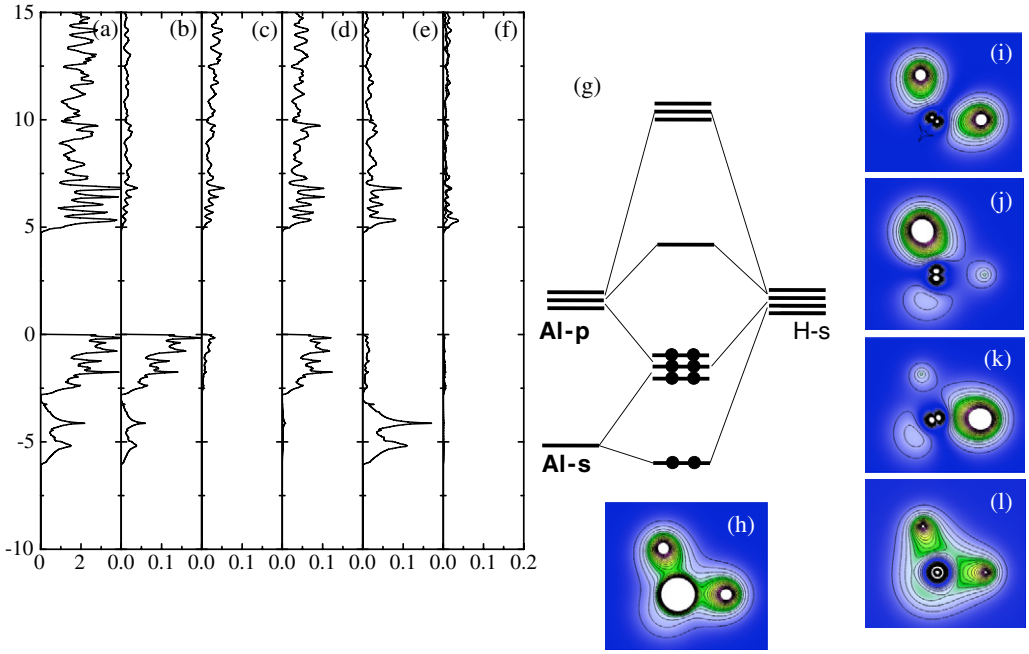


**Figure 7.** (a) Calculated total density of states of $NaAlH_4$ and partial density of states of $NaAlH_4$: (b) H s, (c) Al d, (d) Al p, (e) Al s, (f) Na s, p. The energy zero is set to be at the valence band maximum. (g) Molecular orbitals of $AlH_4$. Dots represent electrons occupying the molecular orbitals in the case of an eight-electron system like $CH_4$. (h) Total charge density of $(AlH_4)^-$ molecule and (h)–(k) represent each molecular orbital of an isolated $(AlH_4)^-$.

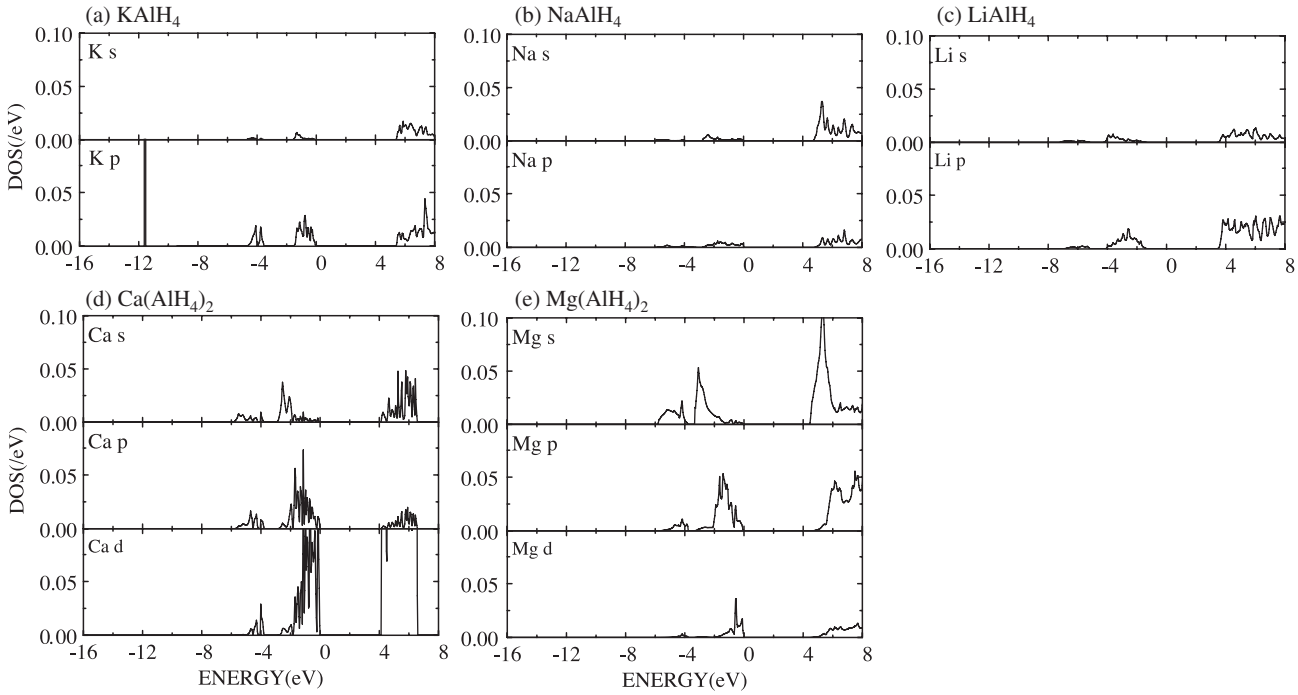


**Figure 8.** Cation partial DOS of alanates with different cations. The energy zero is set to be at the valence band maximum. (a) $KAlH_2$, (b) $NaAlH_4$, (c) $LiAlH_4$, (d) $Ca(AlH_4)_2$, (e) $Mg(AlH_4)_2$.

square planar geometry. The distortion causes splitting of the triply degenerated states in the $1t_2$ molecular orbital to doubly degenerated orbitals ($1e_u$) and a non-bonding state ($2a_u$). The bond associated with the $1e_u$ states may become stronger, leading to higher breathing frequency and structural distortion in $AlH_4$.

As mentioned above, in the case of alanates, the breathing modes and bond lengths between Al and H have similar tendencies in relation to the ionization energy of the cation in a similar manner to the amides. However, the bond angles of H–Al–H in our optimized alanate structure do not follow such a trend. Therefore, it is concluded that the

structural and vibrational frequencies in the alanates should be understood not only the effect of the cation hybridization with the particular molecular orbitals but also by direct cation effects due to short bond lengths.

### *4.3. Differences between the amides and alanates*

Differences between the amides and alanates in the electronic structure and the vibration modes remain as an issue to be discussed further. Although the tendency of hybridization between cation orbitals and the molecular orbital in the amides is larger than that in the alanates, stronger tendencies in the vibrational frequencies and structural parameters can be seen in the alanates than in the amides. On this point, two reasons can be considered. As discussed above, in the case of alanates, there are direct effects by cation to hydrogen due to short bond lengths between cation and hydrogen in the structures. The other factor is that, in the amides, the cation orbitals hybridize mostly with the lone-pair $2a_1$ molecular orbital of $NH_2$ while, in the alanates, they hybridize with the $1t_2$ molecular orbitals. As seen in figure 2(i), the components of H s in the molecular orbital of $NH_2$ in the amides is quite small. On the other hand, in the alanates, the amplitude of H s in the $1t_2$ molecular orbital of $AlH_4$ is rather large, as shown in figures 7(i)–(k), leading to more significant influence of the cation on the particular molecular orbital. Therefore, stronger tendencies in the breathing mode frequencies may be found in the alanates than in the amides.

## 5. Conclusion

We have investigated the electronic structure and vibrational modes of the amides and alanates by the first-principles calculation method. We found small but significant tendencies such that the breathing mode frequencies and structural parameters of $NH_2$ in the amides and $AlH_4$ in the alanates vary in accordance with the ionization energy of the cation. The tendency can be explained by the strength in hybridization between cation orbitals and molecular orbitals of $(NH_2)^-$ and $(AlH_4)^-$. We elucidated the microscopic mechanism of correlations between the breathing mode frequencies and the structural parameters by analyzing the calculated electronic structure from a viewpoint of molecular orbitals. For the comparison between the amides and the alanates, stronger trends of the breathing modes can be seen in the alanates than in the amides. This may be due to stronger cation effects in the alanates than in the amides because the amplitude of H s in the particular molecular orbital is much larger.

## Acknowledgments

The authors would like to thank S Hino, H Yamamoto, S Isobe, H Miyaoka, T Nakagawa, N Hanada, T Ichikawa, H Fujii and Y Kojima for invaluable discussions regarding the experimental aspects of hydrogen storage materials. We also thank K Nakada and P Baettig for stimulating discussions on the theoretical aspect. We acknowledge Y Morikawa for providing the STATE code. This work is supported in part by the Grants of the NEDO project 'Advanced Fundamental Research on Hydrogen Storage Materials'. TT acknowledges financial support from a Grant-in-Aid for 'Research Fellow for Young Scientist' by Japan Society for Promotion of Science. The computation in this work has been partly performed using the facilities of the Supercomputer Center at the Institute for Solid State Physics, University of Tokyo and Information Media Center, Hiroshima University.

## References

[1] Schlapbach L and Züttel A 2001 *Nature* **414** 353
[2] Grochala W and Edwards P P 2004 *Chem. Rev.* **104** 1283–316
[3] Akiba E and Iba H 1998 *Intermetallics* **6** 461
[4] Chen P, Xiong Z, Luo J, Lin J and Tan L K 2002 *Nature* **420** 302
[5] Bogdanovi B and Schwickardi M 1997 *J. Alloys Compounds* **253/254** 1
[6] Züttel A, Wenger P, Rentsch S, Sudan P, Mauron P and Emmenegger C 2003 *J. Power Sources* **118** 1
[7] Kadono R, Shimomura K, Satoh K H, Takeshita S, Koda A, Nishiyama K, Akiba E, Ayabe R M, Kuba M and Jensen C M 2008 *Phys. Rev. Lett.* **100** 026401
[8] Hector L G Jr, Herbst J F, Wolf W, Saxe P and Kresse G 2007 *Phys. Rev.* B **76** 014121
[9] Hector L G Jr and Herbst J F 2008 *J. Phys.: Condens. Matter* **20** 064229
[10] Gregory D H 2008 *J. Mater. Chem.* **18** 2321
[11] Tsumuraya T, Shishidou T and Oguchi T 2008 *Phys. Rev.* B **77** 235114
[12] Xiong Z, Keong Yong C, Wu G, Chen P, Shaw W, Karkamkar A, Autrey T, Jones M O, Johnson S R, Edwards P P and David W I F 2007 *Nat. Mater.* **7** 138–41
[13] Aguayo A and Singh D J 2004 *Phys. Rev.* B **69** 155103
[14] Miwa K, Ohba N, Towata S, Nakamori Y and Orimo S 2004 *Phys Rev.* B **69** 245120
[15] Miwa K, Ohba N, Nakamori Y and Orimo S 2005 *Phys. Rev.* B **71** 195109
[16] Filinchuk Y, Yvon K, Meisner G, Pinkerton F and Balogh M 2006 *Inorg. Chem.* **45** 1433–5
[17] Wu H, Zhou W, Udovic T J, Rush J J and Yildirim T 2008 *Chem. Mater.* **20** 1245–7
[18] Rijssenbeek J, Gao Y, Hanson J, Huang Q, Jones C and Toby B 2008 *J. Alloys Compounds* **454** 233
[19] Wu H 2008 *J. Am. Chem. Soc.* **130** 6515–22
[20] Herbst J F and Hector L G Jr 2006 *Appl. Phys. Lett.* **88** 231904
[21] Luo W 2004 *J. Alloys Compounds* **381** 284–7
[22] Leng H Y, Ichikawa T, Hino S, Hanada N, Isobe S and Fujii H 2004 *J. Phys. Chem.* B **108** 8763
[23] Ichikawa T, Leng H, Isobe S, Hanada N and Fujii H 2006 *J. Power Sources* **159** 126–31
[24] Nakamori Y, Kitahara G and Orimo S 2004 *J. Power Sources* **138** 309
[25] Hino S, Ichikawa T, Leng H Y and Fujii H 2005 *J. Alloys Compounds* **398** 62–6
[26] Tokoyoda K, Hino S, Ichikawa T, Okamoto K and Fujii H 2007 *J. Alloys Compounds* **439** 337–41
[27] Orimo S, Nakamori Y, Kitahara G, Miwa K, Ohba N, Noritake T and Towata S 2004 *Appl. Phys.* A **79** 1765
[28] Jin H M and Wu P 2005 *Appl. Phys. Lett.* **87** 181917
[29] Zhang C and Alavi A 2006 *J. Phys. Chem.* B **110** 7139
[30] Linde G and Juza R 1974 *Z. Anorg. Allg. Chem.* **409** 199–214
[31] Kojima Y and Kawai Y 2005 *Chem. Commun.* **395** 236–9
[32] Kojima Y and Kawai Y 2005 *J. Alloys Compounds* **395** 236–9
[33] Bohger J P O, Essmann R R and Jacobs H 1995 *J. Mol. Struct.* **348** 325–8

[34] Franks F (ed) 1972 Liquid water: dielectric properties *Water a Comprehensive Treatise* (New York: Plenum)
[35] Wolverton C and Ozolins V 2007 *Phys. Rev.* B **75** 064101
[36] Sørby M H, Nakamura Y, Bricks H W, Hino S, Fujii H and Hauback B C 2007 *J. Alloys Compounds* **428** 297
[37] David W I F, Jones M O, Gregory D H, Jewell C, Johnson S, Walton A and Edwards P P 2007 *J. Am. Chem. Soc.* **129** 1594–601
[38] Müller M 1996 Anordnung und Dynamik der $NH_2^-$–Ionen in Kalium- und Strontiumamid: Untersuchungenmit Neutronenstreuung *PhD Thesis* University of Kiel
[39] Nagib M, Kistrup H and Jacobs H 1975 *Atomkernenergie* **26** 87–90
[40] Tsumuraya T, Shishidou T and Oguchi T 2007 *J. Alloys Compounds* **446/447** 323
[41] Senker J, Jacobs H, Müller M, Press W, Mayer H M and Ibberson R M 1999 *Z. Anorg. Allg. Chem.* **625** 2025–32
[42] Ravindran P, Vajeeston P, Vidya R, Fjellvag H and Kjekshus A 2006 *J. Power Sources* **159** 88–99
[43] Ozolins V, Majzoub E H and Udovic T J 2004 *J. Alloys Compounds* **375** 1–10
[44] Løvvik O M, Opalka S M, Brinks H W and Hauback B C 2004 *Phys. Rev.* B **69** 134117
[45] Løvvik O M 2005 *Phys. Rev.* B **71** 144111
[46] Løvvik O M and Molin P N 2005 *Phys. Rev.* B **72** 073201
[47] Andersen O K 1975 *Phys. Rev.* B **12** 3060–80
[48] Koelling D D and Arbman G O 1975 *J. Phys. F: Met. Phys.* **5** 2041
[49] Weinert M 1981 *J. Math. Phys.* **22** 2433
[50] Wimmer E, Krakauer H, Weinert M and Freeman A J 1981 *Phys. Rev.* B **24** 864–75
[51] Soler J M and Williams A R 1989 *Phys. Rev.* B **40** 1560–4
[52] Soler J M and Williams A R 1990 *Phys. Rev.* B **42** 9728–31
[53] Hohenberg P and Kohn W 1964 *Phys. Rev.* B **136** 864
[54] Kohn W and Sham L J 1965 *Phys. Rev.* **140** 1133–8
[55] Perdew J P, Burke K and Ernzerhof M 1996 *Phys. Rev. Lett.* **77** 3865–8
[56] Morikawa Y 2001 *Phys. Rev.* B **63** 033405
[57] Morikawa Y, Ishii H and Seki K 2004 *Phys. Rev.* B **69** 041403
[58] Morikawa Y 2005 Simulation tool for atom technology *Introduction to Computational Materials Design—from the Basics to Actual Applications* ed H Kasai, H Akai and H Yoshida (Osaka: Osaka University Press) pp 54–72, 260–73
[59] Nakamoto K 1997 *Infrared and Raman Spectra of Inorganic and Coordination Compounds Part A* 5th edn (New York: Wiley–Interscience)
[60] Hino S, Yamamoto H, Ichikawa T and Kojima Y 2008 private communications
[61] Sansonetti J E, Martin W C and Young S L 2005 *NIST Handbook of Basic Atomic Spectroscopic Data* (Gaithersburg, MD: Physics Laboratory, National Institute of Standards and Technology)
[62] Herbst J F and Hector L G Jr 2005 *Phys. Rev.* B **72** 125120
[63] Gomes S, Renaudin G, Hagemann H, Yvon K, Sulic M P and Jensen C M 2005 *J. Alloys Compounds* **390** 305–13
[64] Yukawa H, Morisaku N, Li Y, Komiya K, Rong R, Shinzato Y, Sekine R and Morinaga M 2007 *J. Alloys Compounds* **446/447** 242–7
[65] Komiya K, Morisaku N, Shinzato Y, Ikeda K, Orimo S, Ohki Y, Tatsumi K, Yukawa H and Morinaga M 2007 *J. Alloys Compounds* **446/447** 237–41